Review
Graphite

D. D. L. CHUNG
*Composite Materials Research Laboratory, State University of New York at Buffalo,
Buffalo, NY 14260-4400, USA*
E-mail: ddlchung@acsu.buffalo.edu

Graphite is reviewed in terms of its physics and chemistry, with particular attention on its physical properties, intercalation compounds, exfoliated form, activated form, fibers and oxidation protection. © *2002 Kluwer Academic Publishers*

1. Introduction

Carbon is polymorphic. It exists in three forms, namely diamond, graphite and fullerenes. The main difference between diamond and graphite is that the carbon bonding involves sp^3 (tetrahedral) hybridization in diamond and sp^2 (trigonal) hybridization in graphite. As a result, diamond has a three-dimensional crystal structure (covalent network solid), whereas graphite consists of carbon layers (with covalent and metallic bonding within each layer) which are stacked in an AB sequence (different from the AB sequence in a hexagonal close packed or HCP crystal structure) and are linked by a weak van der Walls interaction produced by a delocalized π-orbital. The carbon layers in graphite are known as graphene layers.

Graphite is anisotropic, being a good electrical and thermal conductor within the layers (due to the in-plane metallic bonding) and a poor electrical and thermal conductor perpendicular to the layers (due to the weak van der Waals forces between the layers). The electrical conductivity enables graphite to be used as electrochemical electrodes and as electric brushes for (due to the in-plane covalent bonding) and weak perpendicular to the layers. As a result of this anisotropy, the carbon layers can slide with respect to one another quite easily, thus making graphite a good lubricant and pencil material.

Due to the anisotropy, graphite is able to undergo chemical reactions by allowing the reactant (called the intercalate) to reside between the graphene layers, forming compounds (called intercalation compounds) [1, 2]. Such reactions are known as intercalation. A graphite intercalation compound (GIC) in which there is charge transfer between the intercalate and graphite tends to be more conductive electrically than graphite. The conductivity leads to high effectiveness for electromagnetic interference (EMI) shielding [3]. Most GICs can be exfoliated upon heating [4]. Compression of exfoliated graphite flakes without a binder results in mechanical interlocking, thus forming a flexible and resilient sheet known as flexible graphite—a gasket material [5].

Amorphous carbon usually refers to carbon which has bonding and structure similar to graphite, except that there is no long-range order. The AB stacking order is absent and the layers are usually not flat. Upon heat treatment, amorphous carbon increases its degree of crystallinity (called degree of graphitization). Numerous carbons used in practice, such as carbon fibers, are not totally graphitic, but have a wide gradation of different degrees of graphitization, depending on the heat treatment temperature.

Carbon fibers have a preferred orientation (a crystallographic texture known as the fiber texture) such that the carbon layers are preferentially parallel to the fiber axis, even though the layers tend to be not flat. As a result, carbon fibers are mechanically strong and conducting (electrically and thermally) along the fiber axis. Carbon fibers are widely used as a reinforcement in polymer-matrix composites for lightweight structures.

2. Structure

Graphite has a layer structure in which the atoms are arranged in a hexagonal pattern within each layer and the layers are stacked in the AB sequence [6]. This results in a hexagonal unit cell with dimensions $c = 6.71$ Å and $a = 2.46$ Å [7]. There are 4 atoms per unit cell, as labelled by A, A', B and B' in Fig. 1. The atoms A and B are on one layer plane and the atoms A' and B' are on a layer plane displaced by half the crystallographic c-axis spacing, i.e., 3.35 Å. The atoms A and A' differ from the atoms B and B' in that the A and A' atoms have neighbors directly above and below in adjacent layer planes whereas the B and B' atoms do not. The crystal structure corresponds to the space group $P6_3/mmc$ or [8, 9], in which the 6_3 screw axis is a consequence of the AB stacking. The structure possesses a center of inversion symmetry at the point half way between the atoms A and A'.

The translation vectors of the graphite crystal structure, as shown in Fig. 2, are
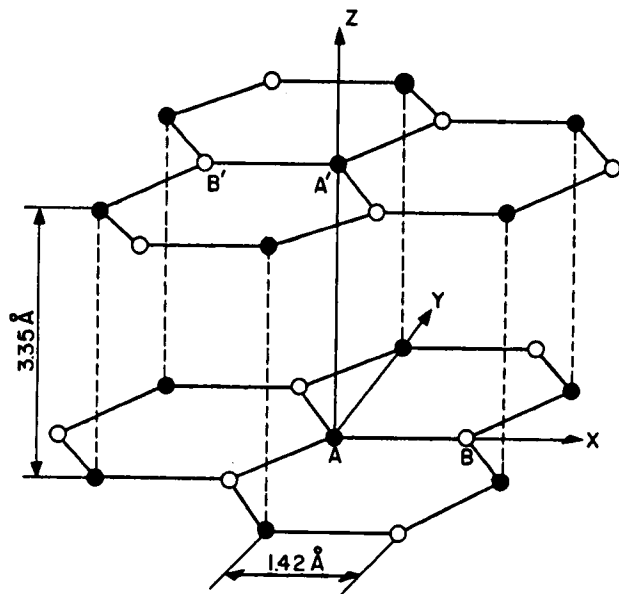
Figure 1 The crystal structure of graphite. The primitive unit cell is hexagonal, with dimensions $a = 2.46$ Å and $c = 6.71$ Å. The in-plane bond length is 1.42 Å. There are four atoms per unit cell, namely A, A′, B and B′. The atoms A and A′, shown with full circles, have neighbors directly above and below in adjacent layer planes; the atoms B and B′, shown with open circles, have neighbors directly above and below in layer planes 6.71 Å away.
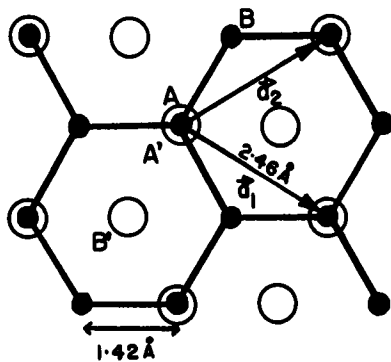

Figure 2 In-plane structure of graphite. The layer plane shown contains atoms A and B (●). The positions of the atoms A′ and B′ (○) on the adjacent layer plane are also shown. The lattice translation vectors on a layer plane are $\vec{a_1}$ and $\vec{a_2}$.

$$\vec{a_1} = a(\sqrt{3}/2, -1/2, 0), \quad |\vec{a_1}| = a = 2.46\,\text{Å}$$

$$\vec{a_2} = a(\sqrt{3}/2, -1/2, 0), \quad |\vec{a_2}| = a = 2.46\,\text{Å}$$

$$\vec{a_3} = c(0, 0, 1), \quad |\vec{a_3}| = c = 6.71\,\text{Å}$$

These vectors are indicated in terms of the orthonormal coordinates (x, y, z).

The in-plane lattice parameter is $a = \sqrt{3}a_0$, where $a = 1.42$ Å, the in-plane nearest neighbor distance.

The out-of-plane lattice parameter is $c = 2c_0$, where $c = 3.35$ Å, the distance between atoms A and A′ on adjacent layer planes. Thus a direct lattice vector is

$$\vec{R_n} = n_1\vec{a_1} + n_2\vec{a_2} + n_3\vec{a_3}$$

$$= a\left(\frac{\sqrt{3}}{2}(n_1 + n_2), \frac{a}{2}(-n_1 + n_2), cn_3\right)$$

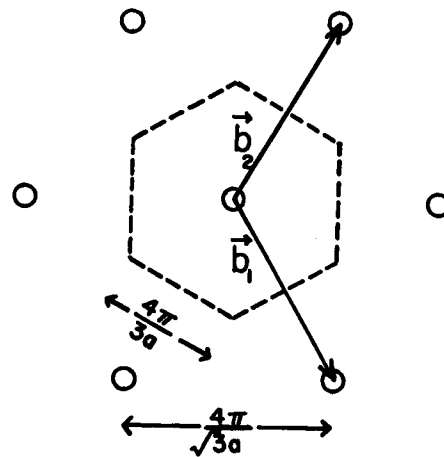where n_1, n_2 and n_3 are integers.

Figure 3 Graphite reciprocal lattice plane generated by basis vectors $\vec{b_1}$ and $\vec{b_2}$. The first Brillouin zone is indicated by the dashed lines.

The translation vectors $\vec{a_1}$, $\vec{a_2}$, $\vec{a_3}$ correspond to a reciprocal lattice with basis vectors

$$\vec{b_1} = \frac{2\pi}{a}\left(\frac{1}{\sqrt{3}}, -1, 0\right), \quad |\vec{b_1}| = \frac{2\pi}{a}\frac{2}{\sqrt{3}}$$

$$\vec{b_2} = \frac{2\pi}{a}\left(\frac{1}{\sqrt{3}}, 1, 0\right), \quad |\vec{b_2}| = \frac{2\pi}{a}\frac{2}{\sqrt{3}}$$

$$\vec{b_3} = \frac{2\pi}{c}(0, 0, 1), \quad |\vec{b_3}| = \frac{2\pi}{c}$$

The reciprocal lattice plane, generated by $\vec{b_1}$ and $\vec{b_2}$, is shown in Fig. 3.

A reciprocal lattice vector is

$$\vec{G}_m = m_1\vec{b_1} + m_2\vec{b_2} + m_3\vec{b_3}$$

$$= \left(\frac{2\pi}{\sqrt{3}a}(m_1 + m_2), \frac{2\pi}{a}(m_1 - m_2), \frac{2\pi}{c}m_3\right)$$

where m_1, m_2, m_3 are integers.

There are four atoms per unit cell, namely atoms A, B, A′ and B′, as indicated in Fig. 3. The coordinates are

$$\vec{\rho_A} = (0, 0, 0),$$

$$\vec{\rho_B} = \frac{a}{2}\left(\frac{1}{\sqrt{3}}, 1, 0\right),$$

$$\vec{\rho_{A'}} = \left(0, 0, \frac{c}{2}\right),$$

$$\vec{\rho_{B'}} = \left(-\frac{a}{2\sqrt{3}}, -\frac{a}{2}, \frac{c}{2}\right)$$

for atoms, A, B, A′ and B′ respectively.

The structure factor is given by

$$A_s(\vec{G}_m) = \underline{SA}\sum_j e^{-i\vec{G}_m\cdot\vec{\rho_j}}$$

where $\underline{S}$ is the scattering efficiency and $\underline{A}$ is the amplitude of the incident wave. Thus for graphite, the structure factor is

$$A_s(\vec{G}_m) = \underline{SA}\left[1 + e^{-i\frac{2\pi}{3}(2m_1 - m_2)}\right] \cdot [1 + e^{-i\pi m_3}]$$
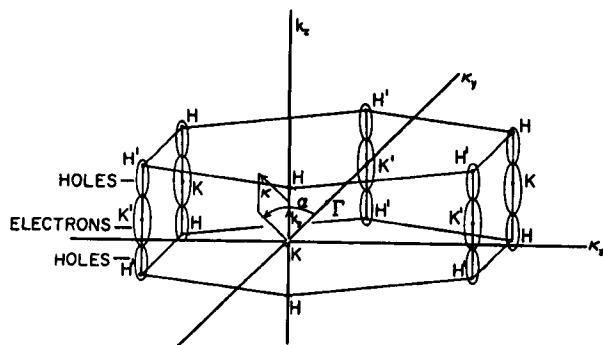
Figure 4 The conventional Brillouin zone of graphite. The electron and hole Fermi surfaces are located in the vicinity of the edges HKH and H'K'H'.

Hence, $A_s(\overrightarrow{G_m}) = 0$ for m_3 = odd integer, and there is no Bragg reflection for m_3 = odd integer, consistent with the consequence of the 6_3 screw axis along the $\overrightarrow{a_3}$ direction. As a result, the first Brillouin zone is formed by the planes $k_z = \pm\frac{2\pi}{c}$ and the six planes going through the dashed segments shown in Fig. 3. Thus the first Brillouin zone is a hexagonal prism with a height of $\frac{4\pi}{c}$. However it is usually drawn with height $\frac{2\pi}{c}$, as shown in Fig. 4, where the planes $k_z = \pm\frac{\pi}{c}$ are not true Brillouin zone boundaries.

In addition to the hexagonal structure described above, there is a less frequent form of graphite in which the carbon layers are stacked in the sequence ABC, resulting in a rhombohedral structure [10, 11]. The carbon layer spacing and the a-axis parameters are the same in both the hexagonal and rhombohedral structures. In the rhombohedral structure, the center of a carbon hexagon in the A layer is dirctly below a corner of a hexagon in the B layer, which is in turn directly below an inequivalent corner of a hexagon in the C layer. The electron energy band structure of rhombohedral graphite has been calculated [12, 13]. The dispersion with the component of the wave vector parallel to the c-axis causes a band overlap of ~0.02 eV. Thus, according the McClure, above ~150 K, the properties of rhombohedral graphite in the plane perpendicular to the c-axis are almost the same as those of two-dimensional graphite. At low temperatures, the behavior is that of a "smeared" two-dimensional band structure. Grinding introduces the rhomobohedral phase [14–16].

Most of the fundamental research on graphite has been carried out on natural single crystal graphite or pyrolytic graphite. The former occurs as flakes of 1 or 2 mm in diameter, embedded in calcite stones. To separate the graphite flakes from the stone, chemical methods have usually been employed, by which the stone is immersed in boiling acids (HCl and HF) [17]. Pyrolytic graphite, on the other hand, is synthetic. However, its properties are similar to those of single crystal graphite and its large size is an advantage in many experimental measurements.

Pyrolytic graphite (PG) is polycrystalline, having a fiber texture such that the c-axis of all the crystallites are aligned but the a-axes are random. It is formed by pyrolysis, in which a carbonaceous gas, such as hydrocarbons, is cracked generally on a graphite substrate above 2000°C. This process results in crystallites having their c-axes predominantly normal to the substrate

(mosaic spread = 40–50°) and a density of more than 2.2 g/cm³. To improve the crystallite alignment, stress recrystallization is used. This involves hot-pressing with uniaxial pressures of 300–500 kg/cm² at 2800–3000°C and produces specimens more than 10 mm thick along the c-axis and a density of 2.266 g/cm³, more than 99.95% of the theoretical density. Subsequent annealing of such material at 3400–3500°C under a light load yields highly-oriented pyrolytic graphite (HOPG) with a mosaic spread of 0.02°C and a crystallite size of the order of 1 μm in both a and c directions [18].

It should be noted that pyrolytic graphite available before ~1960 was not highly-oriented, so that experimental results on such materials should be treated with caution.

3. Bonding

An isolated carbon atom has an electronic configuration of $1s^2 2s^2 2p^2$. The $1s^2$ electrons belong to the ion core and the remaining four electrons are valence electrons. In graphite, the 2s, $2p_x$ and $2p_y$ electrons form three sp^2 hybridized orbitals directed 120° apart on a layer plane. Overlap of these orbitals leads to the formation of σ-bonding between carbon atoms on a layer plane. The $2p_z$ electron, on the other hand, forms a delocalized orbital of π symmetry. This delocalization stabilizes the in-plane carbon bonding so that the bond strength is higher than that of a single covalent C–C bond. In addition, the delocalization results in loosely bound π-electrons of high mobility, so that the π-electrons play a dominant role in the electronic properties of graphite. The carbon layers are bound in the c-direction by weak van der Waals forces. As a result, graphite is anisotropic, having different physical properties for in-plane and c-axis crystallographic directions.

4. Electronic energy band structure

In graphite, each carbon atom has four valence electrons and there are four atoms per unit cell. Therefore, there are 16 energy bands (not counting spin), of which 12 are σ-bands and 4 are π-bands. Six σ-bands are bonding and six at higher energies are anti-bonding. These 2 groups of six σ-bands are separated by ~5 eV. The π-bands lie between these two groups of σ-bands. Similarly, two π-bands are bonding and two are anti-bonding. However all bands are coupled and the four π-bands are strongly coupled. Since graphite has 16 electrons per unit cell, only 8 energy bands are filled. Thus the Fermi level lies in the middle of the four π-bands. The upper π-bands, which form the highest valence bands, overlap along the Brillouin zone edges HKH and H'K'H', making graphite a semi-metal. The band overlap energy is about 0.03 eV. The energy bands can be illustrated in one dimension as shown in Fig. 5.

In three dimensions, the energy bands are shown in Fig. 6. Along the HKH and H'K'H' axes, the four π-bands are labeled E_1, E_2 and E_3, where the E_3 band is doubly degenerate along the zone edges. The E_1 band is empty. The E_2 band is nearly full and defines the minority hole pocket near the zone corner. The E_3 band
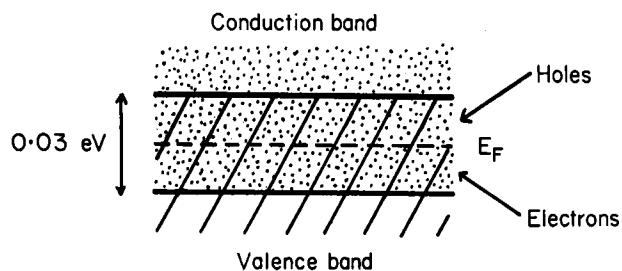
3

Figure 5 One-dimensional energy bands of graphite. The valence (■) and conduction bands (▩) have an overlap of 0.03 eV. The Fermi energy (E_F^0) lies within the band overlap region, resulting in pockets of holes and electrons.
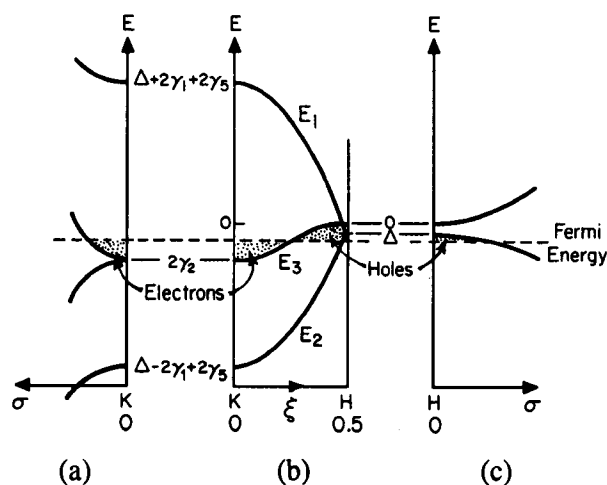

(a)   (b)   (c)

Figure 6 Three-dimensional energy bands of graphite, showing schematically the wave vector (ξ, σ) dependence of the energy (E) of the graphite π-bands. The dashed line represents the Fermi level (E_F^0) for pure graphite. (a) Energy vs dimensionless wave vector σ in the plane $\xi = 0$ about the K point. (b) Energy vs dimensionless wave vector ξ along the edges HKH and H′K′H′. (c) Energy vs σ in the plane $\xi = 1/2$ about the H point.

is partly occupied and defines the majority electron and hole carrier pockets. The wave vector coordinates shown are ξ and σ, where ξ is the dimensionless wave vector along the c-axis and is related to the wave vector k_z, measured from the K point, by

$$\xi = k_z c_0 / 2\pi.$$

The other coordinate σ is the dimensionless wave vector in the basal plane and is related to the wave vector κ measured from the zone edge by

$$\sigma = \frac{1}{2}\sqrt{3}a\kappa$$

The dimensionless wave vectors σ and ξ, together with the basal plane polar angle α completely specify the cylindrical coordinate system, which is shown in Fig. 4.

The E_3 band lies very close to the Fermi energy (E_F) and forms carrier pockets along the HKH axis. The three pockets, two of which contain holes and one of which contains electrons, are shaded in Fig. 6. The Fermi energy is chosen so that the volumes of the electron and hole pockets are equal. The degeneracy of the E_3 band is lifted away from the zone edge as one moves in the

basal plane, except at the planes $\xi = 1/2$. The regions around the zone edges are the only parts of the Brillouin zone where bands cross the Fermi energy. Therefore all of the free carriers are located along the zone edges, giving rise to slender Fermi surfaces along these edges, as shown in Fig. 4. A Fermi surface extends less than 1% of the distance from the zone edge to the zone center. Half of one Fermi surface, between the H point and the K point, is shown in Fig. 7. It consists of one hole pocket and half of an electron pocket. The hole pocket and the electron pocket are connected at four points; three, known as "legs", are off the HKH axis; one, known as "central", is on the HKH axis.

It can be seen from Fig. 7 that the cap or top portion of the majority hole Fermi surface protrudes beyond the H point. Thus, translation by a reciprocal lattice vector of the cap portion results in a minority hole surface in the vicinity of the H point, as shown in the extended zone scheme in Fig. 8.

GRAPHITE FERMI SURFACE MODEL
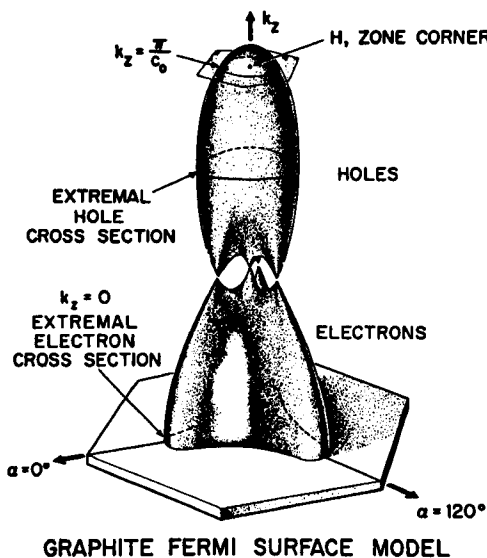
Figure 7 Fermi-surface model for graphite, showing extremal cross sections which correspond to the constant-energy orbits normal to the k_z direction.

(a) NO SPIN-ORBIT INTERACTION   (b) WITH SPIN-ORBIT INTERACTION

Figure 8 Fermi surface for minority holes near the Brillouin zone corner (the H point) shown in the extended zone scheme. This surface is formed by the overlap of the portions of the Fermi surface which extend beyond the planes $\xi = \pm 1/2$. The extremal cross section around the H point and perpendicular to the c-axis is indicated.

5. Energy band model

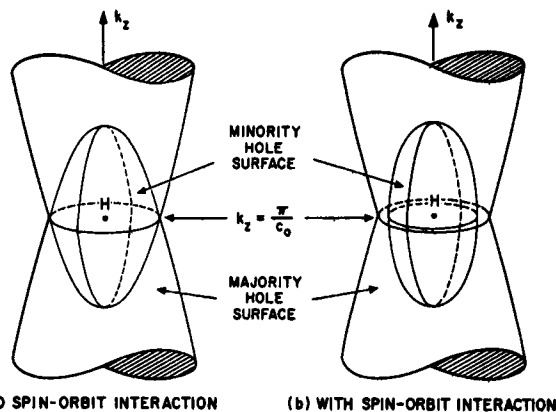Slonczewski and Weiss [19] developed an energy band model describing the electronic energy dispersion relations for the region of the Brillouin zone around the HKH axis. The energy dependence along the k_z direction (HKH) is determined by a Fourier expansion in ξ. Since the interlayer binding is weak, the Fourier series should be rapidly convergent and only a few terms need to be retained. In the basal plane, $\vec{k} \cdot \vec{p}$ perturbation theory is used to expand the Hamiltonian in terms of $\vec{k}$, a wave vector in the k_x k_y plane measured from the zone edge, taking the zero-order wave-function as those at the vertical edge HKH of the Brillouin zone. Because of small dimensions of the Fermi surface in the k_x and k_y directions, the $\vec{k} \cdot \vec{p}$ expansion will converge rapidly. Symmetry is used to determine the minimum number of independent parameters.

The effective mass Hamiltonian of the Slonczewski-Weiss-McClure (S-W-McC) band model is customarily written as [19, 20]:

$$H = \begin{pmatrix} E_1 & 0 & H_{13} & H_{13}^* \\ 0 & E_2 & H_{23} & -H_{23}^* \\ H_{13}^* & H_{23}^* & E_3 & H_{33} \\ H_{13} & -H_{23} & H_{33}^* & E_3 \end{pmatrix}$$

where

$$E_1 = \Delta + \gamma_1 \Gamma + \frac{1}{2}\gamma_5 \Gamma^2,$$

$$E_2 = \Delta - \gamma_1 \Gamma + \frac{1}{2}\gamma_5 \Gamma^2,$$

$$E_3 = \frac{1}{2}\gamma_2 \Gamma^2,$$

$$H_{13} = -\gamma_0(1 - v)\sigma e^{i\alpha}/2^{1/2},$$

$$H_{23} = \gamma_0(1 + v)\sigma e^{i\alpha}/2^{1/2},$$

$$H_{33} = \gamma_3 \Gamma \sigma e^{i\alpha},$$

$$\Gamma = 2\cos(\pi \xi),$$

and

$$v = \gamma_4 \Gamma / \gamma_0.$$

Once the seven band parameters (Δ, γ_0, γ_1, γ_2, γ_3, γ_4, γ_5) are specified, the energy bands near the zone edge and the Fermi surface are completely determined. Shown in Table I are the values of the band parameters, chosen [21] to provide a good fit to the K-point [22, 23] and H-point [24] magnetoreflection spectra, as well as to the majority and minority de Haas-van Alphen periods [25, 26].

The eigenvalues of the Hamiltonian H give the energy dispersion relations. Along the zone edge HKH, two of the four solutions are doubly degenerate and correspond to E_3. The remaining two solutions are nondegenerate and correspond to E_1 and E_2 in Fig. 6. At the H point ($\xi = 1/2$), E_1 and E_2 become degenerate and the double degeneracy of these levels and of the E_3 levels is maintained as one moves away from the H point in the plane $\xi = 1/2$, as is shown in Fig. 6c.

TABLE I Electronic energy band parameters of graphite

Parameter	Value (eV)	Physical origin
γ_0	3.12	Overlap of neighboring atoms in a single layer plane
γ_1	0.377	Overlap of orbitals associated with A and A' atoms located one above the other in adjacent layer planes
γ_2	−0.0206	Interactions between atoms in next nearest layers and from coupling between π and σ bands.
γ_3	0.29	Coupling of the two E_3 bands by a momentum matrix element
γ_4	0.120	Coupling of E_3 bands to E_1 and E_2 bands by a momentum matrix element
γ_5	0.025	Interactions between second nearest layer planes. Introduction in E_1 and E_2 in second order of Fourier expansion to be consistent with E_3
Δ	−0.009	Difference in potential energy at A and B lattice sites.

6. Magnetic energy levels

With the magnetic field along the c-axis, the constant energy orbits are perpendicular to the HKH axis of the graphite Brillouin zone. Corresponding to extrema in the Fermi surface cross-sectional area at different points along the HKH axis, there are three kinds of orbits, as shown in Fig. 9a–c. The orbit shown in Fig. 9a corresponds to the extremal cross section on the majority electron surface at the K point ($k_z = 0$). The orbits shown in Fig. 9b correspond to extremal cross sections on the majority and minority hole surfaces at the H point ($k_z = \frac{\pi}{c_0}$). The outer orbit is on the majority hole surface and the inner orbit is on the minority hole surface. The orbits shown in Fig. 9c, known as leg and central orbits, correspond to extremal cross sections on the majority electron or majority hole surface where the electron and hole surfaces make contact. There are four such contacts; three, known as "legs", are off the HKH axis and the remaining one, known as "central", is on the HKH axis.

There are two approaches to calculate the magnetic energy levels: (i) solution of the effective mass Hamiltonian in the presence of a magnetic field [27–29], (ii) use of the Bohr-Sommerfeld quantization condition [30]. In the first approach, γ_3 is treated in perturbation theory, though γ_3 is actually too large for the use of perturbation theory. In the approximation that $\gamma_3 = 0$, the effective mass magnetic Hamiltonian is much simplified. The solutions of this magnetic eigenvalue problem lead to a set of four Landau ladders, in which the levels are labeled by the index N. The ξ dependence of these ladders is illustrated in the Landau level contour diagram given in Fig. 10 [24]. The second approach is semi-classical, but gives in a straight-forward way the majority levels (resulting from orbits like those shown in Fig. 9a and b) and the special levels (resulting from the leg and central orbits shown in Fig. 9c). The magnetic energy levels at the K point as a function of the magnetic field are shown in Fig. 11. The majority electron Landau levels are cut off at $\varepsilon_{e\text{-sp}}$ while the hole levels are cut off at $\varepsilon_{h\text{-sp}}$. For energies between $\varepsilon_{h\text{-sp}}$
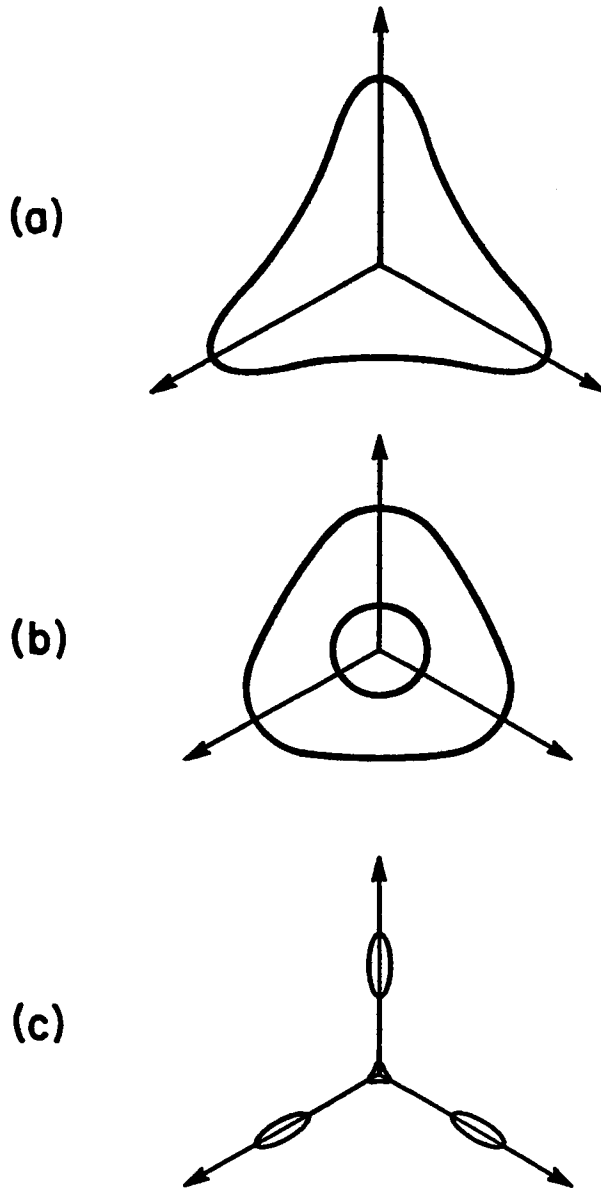
5

(a)

(b)

(c)

Figure 9 Typical constant-energy orbits normal to the HKH axis. (a) Trigonally distorted orbit for majority electrons at the K point. (b) Cap orbits near the H point. The outer orbit is for the majority holes; the inner orbit is for the minority holes. (c) Leg and central orbits near the confluence of the electron and hole surfaces.

and $\varepsilon_{e\text{-sp}}$, the special levels (sp) exist. At higher magnetic fields only the field independent levels $n_{\text{leg}} = 0$ and $n_c = 0$ exist in the special level energy range. Interband transitions from one of the central or leg levels to one of the majority levels are possible. The $n_{\text{leg}} = 0$ and $n_c = 0$ levels serve as initial states over a wide range of magnetic fields. Therefore "ℓ" or "leg" is used to designate the leg level $n_{\text{leg}} = 0$ and "c" or "central" is used to designate the central level $n_c = 0$.

7. Electrical properties

The electrical conductivities (σ_a, σ_c), mobilities (μ_a, μ_c), relaxation times (τ_a, τ_c), mean free paths (ℓ_a, ℓ_c) and electron density (n) at various temperatures for pyrolytic graphite are shown in Table II [31], for which $m_a^* = 0.05 m_0$, $v_a = 2 \times 10^7$ cm/s, $m_c^* = 6 m_0$ and $v_c = 10^6$ cm/s for computation purposes.

Due to the difficulty in measuring the intrinsic c-axis conductivity, the value of σ_a/σ_c is subject to
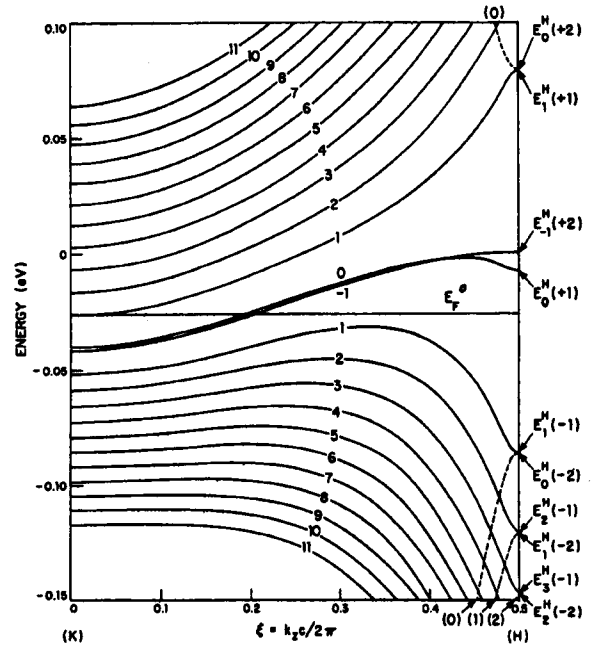
Figure 10 Graphite Landau levels labeled by N along the KH axis for $H = 50$ kG and $\gamma_3 = 0$. The levels at the H-point are labeled by a Landau level quantum number and a ladder index. The Landau levels of the E_1 and E_2 bands are shown as dashed curves. The Fermi level (E_F^0) for pure graphite is indicated by a horizontal line.
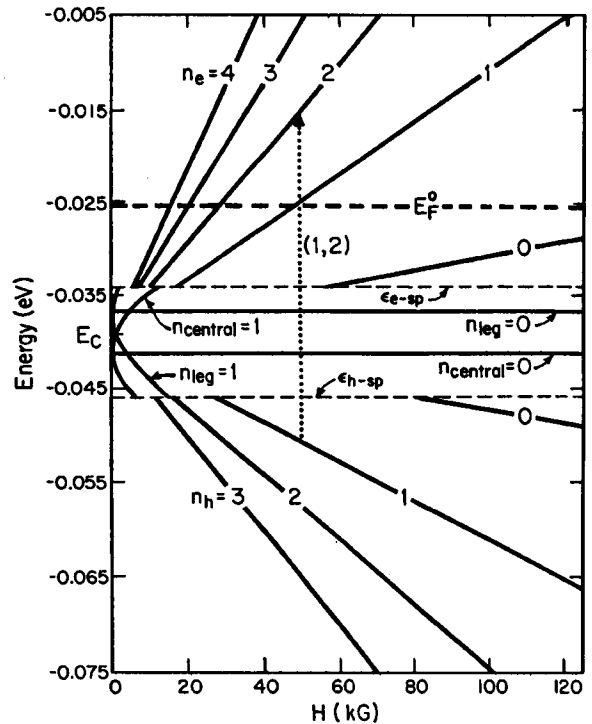
Figure 11 The magnetic field dependence of the Landau levels at the K point. The majority Landau levels labelled by the index n_e for the conduction band and the index n_h for the valence band are cut off respectively at energies labelled by $\varepsilon_{e\text{-sp}}$ and $\varepsilon_{h\text{-sp}}$, between which are the "leg" Landau levels and the "central" Landau levels labelled by the indices n_{leg} and n_{central} respectively. The interband Landau level transition from $n_h = 1$ to $n_e = 2$ labelled by (1, 2) is indicated on the figure at a magnetic field $H = 50$ kG. The Fermi energy for pure graphite is indicated by E_F^0.

controversy. The reported anisotropy ratio is 10^2–10^4 in single crystal graphite and 10^3–10^5 in pyrolytic graphite [25]. The reason for this difference has not been well understood.

TABLE II [a]Electrical properties of graphite

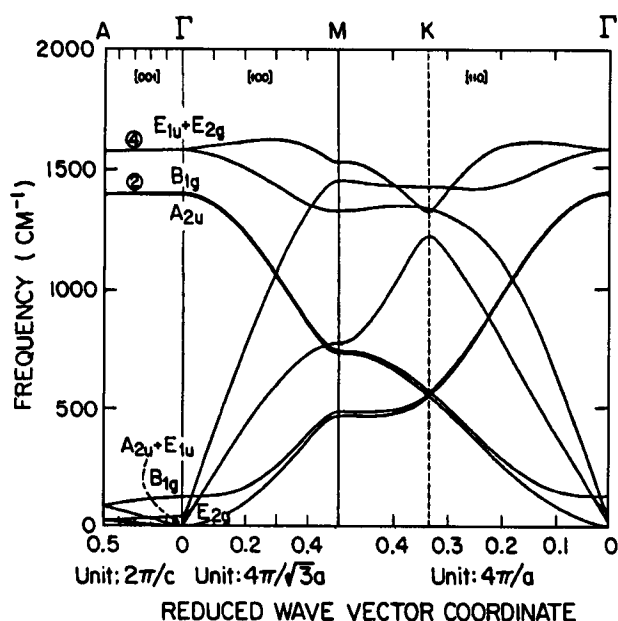|		300 K	77.5 K	4.2 K
σ_a	$(10^4\ ohm^{-1}\ cm^{-1})$	2.26	3.87	33.2
σ_c	$(ohm^{-1}\ cm^{-1})$	5.9	3.3	3.8
σ_a/σ_c	(10^4)	0.38	1.2	8.8
μ_a	$(10^4\ cm^2/V.s)$	1.24	5.75	7.0
μ_c	$(cm^2/V.s)$	3.3	5.0	8.0
τ_a	$(10^{-13}\ s)$	3.5	16.2	196
τ_c	$(10^{-14}\ s)$	0.95	1.6	2.7
ℓ_a	$(10^3\ \text{Å})$	0.7	3.2	39
ℓ_c	(Å)	0.95	1.6	2.7
n	$(10^{18}\ cm^{-3})$	11.3	4.2	3.0

[a] Ref. [32].

Figure 12 Phonon dispersion relation for graphite in the [001], [100] and [110] directions, according to Nicklow *et al.* (1972).

The Hall coefficient is ~ -0.1 cm^3/coulomb in pyrolytic graphite at room temperature for magnetic fields ≤ 10 kG.

8. Lattice properties

The lattice modes of graphite have been studied by Raman scattering [9, 32, 33], infrared spectroscopy [9, 32, 34] and neutron scattering [35]. Phonon dispersion relation in the [001], [100] and [110] directions, as calculated from neutron scattering results, is shown in Fig. 12. The symmetry assignment of each curve is indicated in the figure. The optical phonon modes near the zone center (Γ-point) have been studied by Raman scattering and infrared spectroscopy.

The optical lattice vibrational modes of graphite are shown in Fig. 13. The E_{2g_1} and E_{2g_2} modes are Raman active. The E_{1u} and A_{2u} modes are infrared active. The B_{1g_1} and B_{1g_2} modes are silent. The interlayer phase difference between the E_{1u} and E_{2g_2} modes indicates that the frequency difference between these two modes (~ 10 cm^{-1}) is a measure of the interlayer force constant of the graphite lattice.

The E_{2g_1} and E_{2g_2} modes have been studied by using Raman scattering [36]. The E_{2g_2} mode has been observed at 1582 ± 2 cm^{-1} in highly-oriented pyrolytic
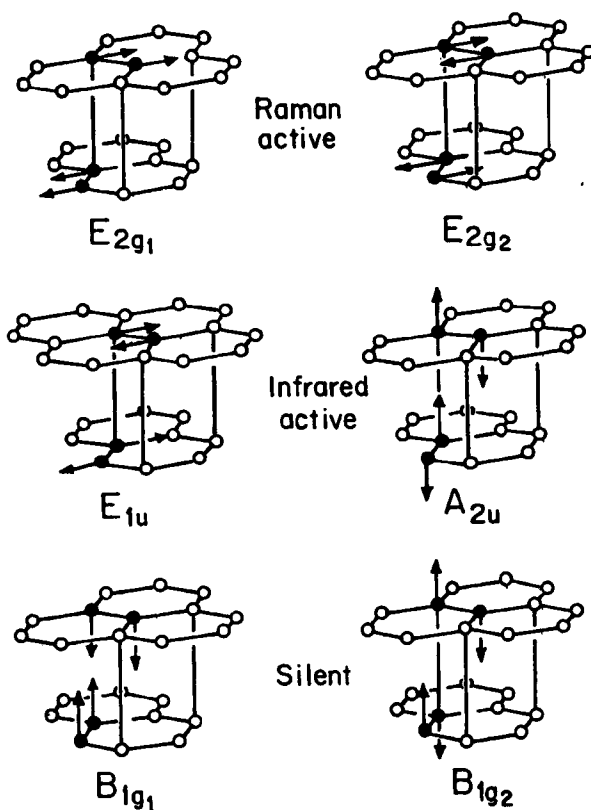
Optical Eigenmodes of Graphite

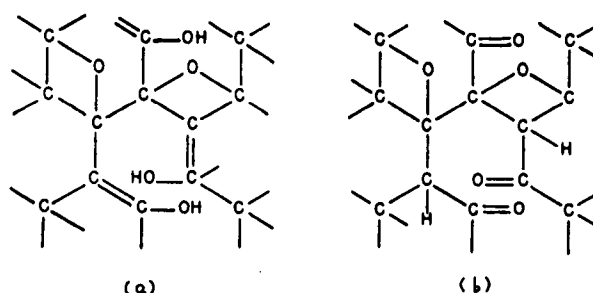*Figure 13* Optical lattice vibrational modes of graphite.

Figure 14 Structure of graphite oxide proposed by Clauss *et al.* (1957). (a) enol form, (b) keto form.

graphite [32, 37], with a halfwidth of ~ 14 cm^{-1}. This frequency is quite close to the C–C vibrational frequency (1584.8 cm^{-1}) in the benzene molecule [38]. The second order (two phonon) Raman line of E_{2g_2} has been observed at 3248 cm^{-1}; this peak is upshifted by 86 cm^{-1} from $2\omega_R$, where $\omega_R = 1581$ cm^{-1} is the first order Raman frequency [39]. The second order line is narrower than and 40% as intense as the first order one. These observations were interpreted in terms of ordinary overtone scattering. Much less is known concerning the E_{2g_1} mode. It has been estimated theoretically that the E_{2g_1} mode is at ~ 210 cm^{-1} [9]. Unpublished work indicates that the E_{2g_1} mode has been observed at 140 ± 10 cm^{-1} with a halfwidth of 40 cm^{-1} and is two orders of magnitude weaker than the E_{2g_2} mode [32].

In less perfect graphite materials, such as commercial graphite or charcoal, a Raman line at 1355 cm^{-1}

has been observed [33]. This line may be related to the tetrahedral bonding in the diamond structure, since diamond has a Raman peak at $1322 \, cm^{-1}$.

The E_{1u} and A_{2u} modes have been studied by using infrared reflection spectroscopy. With the electric field $E \perp c$, the E_{1u} mode has been observed at room temperature at $1588 \pm 5 \, cm^{-1}$ in single crystal graphite [32], with a halfwidth of $\sim 15 \, cm^{-1}$. With $E \perp c$, the E_{1u} mode has also been observed at room temperature in highly-oriented pyrolytic graphite at $1588 \, cm^{-1}$ [39]. With $E // c$, the A_{2u} mode has been observed at room temperature at $868 \pm 1 \, cm^{-1}$ in highly-oriented pyrolytic graphite [39]. A mechanically polished a-face was used for measurements with $E // c$. The macroscopic effective charges for the E_{1u} and A_{2u} modes have been calculated to be 0.41 e and 0.11 e respectively [39].

9. Graphite intercalation compounds
9.1. Graphite compounds

Graphite reacts with many chemical substances to form compounds. Graphite compounds can be classified into three groups, namely surface compounds, substitutional compounds and intercalation compounds.

The surface compounds of graphite [40] are formed by the reaction with the graphite surface atoms. Adsorption occurs on the planar surfaces perpendicular to the c-axis as well as on the edge atoms of the carbon planes. Because of the free valence bonds of the edge atoms, the edge atoms tend to be more active. The oxidation reaction is an example of a surface reaction.

The substitution compounds of graphite [40] contain the foreign species substitutionally.

The intercalation compounds of graphite [41–45] are interstitial compounds in which the foreign species is included in the interplanar interstitial sites of the graphite crystal such that the layer structure of the graphite lattice (Fig. 1) is retained. These compounds are the most well-known of all the compounds of graphite.

9.2. Classification of graphite intercalation compounds

In graphite, the carbon atoms within a layer are strongly bound by electronic σ-bonds and the carbon atoms in adjacent layers are weakly bound by electronic π-bonds. As a result, the intercalating substance (or intercalate) occupies and thereby expands the interplanar spacing of the graphite crystal without disrupting the carbon layers. The intercalation process in graphite is chemical as well as physical in nature. The kind of interaction or bonding between the carbon atoms and the intercalate depends on the particular intercalate. According to the character of the bonding, the intercalation compounds of graphite can be classified into two groups.

The first group, in which the bonding is covalent (or homopolar), includes graphite oxide, carbon monofluoride and tetracarbon monofluoride. This type of bonding is favored by the presence of conjugated double bonds within the carbon planes. The layer planes assume a wavy form because of the change of the carbon bonding from the trigonal (sp^2) form to the tetrahedral (sp^3) form. These compounds are non-conducting, lacking the semi-metallic properties of graphite.

The second group, in which the bonding is partially ionic (or polar), includes graphite salts (e.g., graphite nitrate, graphite bisulphate), graphite-alkali metal compounds, graphite-halogen compounds, graphite-metal chloride compounds, etc. It should however be emphasized that the degree of ionicity in compounds of this group may be very low. Moreover, many of the intercalates of this group retain their molecular identity in the graphite lattice, so that the nature of the ionic bonding is more complicated than that in many of the totally ionic solids, where simple ions are involved. Although many of the compounds of this group involve such a small degree of ionization that they should not really be called "ionic", they are referred to as ionic intercalation compounds for convenience in classification. In the presence of excess external intercalate, these compounds have a well ordered interlayer structure. In this state, they are known as lamellar compounds. However when the equilibrium with excess external intercalate is removed, the compounds tend to desorb the intercalate [46, 47]. Although most of the intercalate is lost under such a condition, a fraction is retained even under vacuum or after heating. When the compound has come to equilibrium with a zero partial pressure of external intercalate, it is known as a residue compound [48].

Since pure graphite is a semi-metal, by ionically bonding with the intercalate, the graphite π-bonds can gain electrons from or lose electrons to the intercalate, thereby shifting the position of the Fermi energy from that in pure graphite. In other words, the intercalate atoms can act as donors or acceptors to dope the graphite. The effect on the electronic properties of graphite makes this kind of intercalation compounds interesting.

9.3. Covalent intercalation compounds

Covalent intercalation compounds have received less attention than the ionic ones. The number of known covalent intercalation compounds is also much smaller—only graphite oxide (graphitic acid) and graphite fluorides (carbon monofluroide and tetracarbon monofluoride).

9.3.1. Graphite oxide (graphitic acid)

Graphite oxide is a poorly understood compound. The observation of both the CO stretching mode (which suggests the presence of a keto form) and the OH stretching mode (which suggests the presence of an enol form) suggests that graphite oxide consists of enol, keto and epoxy groups dispersed in the graphite lattice. This structure leads to an idealized empirical formula of $C_8O_2(OH)_2$.

Graphite oxide is an insulator, with an electrical conductivity of 10^3–10^7 $\Omega.cm$ [49], depending on the oxygen content.

9.3.2. Carbon monofluoride (graphite monofluoride)

Graphite-fluorine with an approximate composition of CF [50] is formed by direct reaction of graphite with fluorine at high temperatures or pressures or via a fluorine glow discharge (plasma) [51, 52].

The presence of C–F bonds in carbon monofluoride has been demonstrated by infrared transmission spectroscopy. The presence of CF groups is probably due to excess fluorine, as suggested by the stoichiometry of $CF_{1.12\pm0.03}$. Flourine NMR shows no evidence for mobile fluorine species [45].

These various observations suggest a structure consisting of puckered layers of tetrahedrally coordinated sp^3 hybridized carbon atoms, each covalently bonded to three other carbon atoms and one fluorine atom. X-ray diffraction indicates an interlayer spacing of 5.80 to 6.6 Å [51, 53–55]. According to this model, there are two possible structures. One consists of layers of trans-linked cyclohexane rings in the chair conformation; the other consists of layers of cis-trans-linked cyclohexane boats. X-ray diffraction has not been able to distinguish between the two possibilities. Detailed ^{19}F second-moment studies [53, 56] of the fluorine NMR have provided evidence for a structure consisting of layers of cis-trans-linked cyclohexane rings in the boat conformation.

Carbon monofluoride is an electrical insulator.

9.3.3. Tetracarbon monofluoride

Tetracarbon monofluoride, with an approximate composition of C_4F, is formed by reaction of graphite with F_2 and HF at less than 80°C [43, 51, 57].

The structure of tetracarbon monofluoride differs from that of carbon monofluoride in that the carbon planes are not puckered, as shown by X-ray diffraction [43]. This difference is probably due to the larger number of directional covalent C–F bonds in carbon monofluoride than in tetracarbon monofluoride. The carbon hexagons remain practically the same as in pure graphite, but the graphite planes assume an AA stacking, with an interlayer separation of 5.29 to 5.50 Å [43, 51]. The fluorine atoms are arranged in two layers, one above and one below each carbon layer.

The electrical conductivity of tetracarbon monofluoride is about 100 times smaller than that of pure graphite [58]. However this value is higher than that for carbon monofluoride.

9.4. Ionic intercalation compounds

The majority of graphite intercalation compounds belong to the class in which the bonding between the intercalate and carbon has a certain degree of ionic or polar character. These compounds exist in concentration stages marked by differences in the periodic stacking sequence of the carbon layers and the intercalate layers. The number of carbon layers between two intercalate layers defines the "stage" of the compound. As the concentration of the intercalate increases, the stage decreases. The stages can be identified by X-ray diffraction and by the intercalation isotherms [59], though the

stages can be more clearly distinguished in some compounds than others. Experimental results point to the fact that the bonding in these compounds has some ionic character [58].

These compounds can be formed by the spontaneous interaction of the intercalate with graphite or by electrolysis. The intercalates which form spontaneous intercalation compounds include Br_2, IBr, ICl, K, Rb, Cs, HNO_3, $FeCl_3$, SbF_5, etc. They can be prepared by reacting graphite with the intercalate in liquid or vapor form for hours or days, at temperatures where the vapor pressure of the intercalate is sufficient to overcome the threshold potential for intercalation [60]. Some intercalates can be dissolved in an organic solvent and the compound can then be prepared by immersing the graphite in the solution containing the intercalate. The intercalates which form electrolytic intercalation compounds include NH_3, H_2F_2, H_3PO_4, H_2SO_4, HNO_3, etc. These compounds can be induced to react with graphite by auxiliary oxidizing or reducing agents which do not themselves enter into combination in the resulting compound. This auxiliary agent is most conveniently an external electric battery. For example, graphite bisulphate is formed from the anode when concentrated sulfuric acid is electrolyzed between graphite and a platinum cathode [61, 62]. The majority of the intercalation compounds can be formed spontaneously.

9.4.1. Graphite-halogens

Although many of the properties of the halogens exhibit continuous trends as one considers the elements F, Cl, Br and I down group VII of the periodic table, the reactivity of these halogens towards graphite does not exhibit such a trend. Only fluorine and bromine react readily with graphite; iodine and chlorine do not. However iodine monochloride (ICl) iodine bromide (IBr) and several other interhalogens can be intercalated into graphite.

Several theories have been suggested to account for the varied behavior of the halogens towards graphite. Since the halogens are electronegative, they are expected to accept electrons from the graphite. Experimental results [63] suggest a certain degree of electron transfer from graphite to the halogen intercalate. A high electron affinity and a high polarizability for the intercalate should favor such an interaction. Ref. 64 suggests that, although chlorine and fluorine have high electron affinities, their polarizabilities are low. The reverse is true for iodine. Bromine, on the other hand, apparently exhibits both these properties to a sufficient degree.

Fluorine reacts with graphite but only forms intercalation compounds with covalent bonding, so that the physical properties of graphite-fluorine are quite different from those of the other graphite-halogens.

Graphite-bromine [65, 66] is the most extensively studied of all graphite-halogens. Graphite-bromine lamellar compounds exist in at least four stages (stages 2–5), which have been identified by X-ray diffraction and intercalation isotherm measurements [59].

In determining the isotherms, a known weight of graphite is exposed to a series of bromine vapor pressures from zero to the saturation vapor pressure and
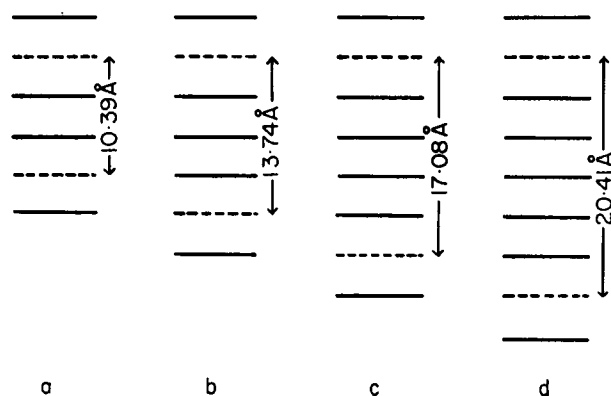
Figure 15 Interlayer ordering in graphite-bromine lamellar compounds of stages 2–5. The dashed lines indicate bromine intercalate layers; the solid lines indicate carbon layers. (a) 2nd stage structure of $C_{16}Br_2$ (6.25 mole % Br_2). (b) 3rd stage structure of $C_{24}Br_2$ (4.17 mole % Br_2). (c) 4th stage structure of $C_{32}Br_2$ (3.13 mole % Br_2). (d) 5th stage structure of $C_{40}Br_2$ (2.50 mole % Br_2).

back to zero, all at the same temperature. For each pressure the equilibrium weight of the sample is determined. The compositions of the phases are indicated by a change in the slope of the isotherm. This isotherm method, in which the pressure is varied at constant temperature, is to be distinguished from the isobar method, in which the temperature of the graphite is varied while holding the pressure constant. The isobar method is usually used for the graphite-alkali metal systems.

The isotherms on pyrolytic graphite show four phases of approximate compositions, $C_{16}Br_2$, $C_{24}Br_2$, $C_{32}Br_2$ and $C_{40}Br_2$, which correspond to stages 2, 3, 4 and 5 respectively (Fig. 15).

When the bromine vapor pressure exceeds the threshold value for the intercalation, the reaction takes place. The concentration of the absorbed bromine increased rapidly with the increase in bromine vapor pressure up to the composition $C_{40}Br_2$. In this range, the intercalate is not distributed homogeneously throughout the graphite crystal as in an ideal dilute solid solution. The diffraction pattern shows the coexistence of regions of the virgin graphite and of regions with the structure of stage 5. When the partial pressure of bromine is about 0.15, the structure becomes a homogeneous 5th stage structure of composition $C_{40}Br_2$. With further increase of bromine vapor pressure, the structure follows the stages of higher bromine concentrations one by one, up to the 2nd stage structure of saturation. At intermediate bromine concentrations between the definite compositions corresponding to definite stages, the X-ray diffraction pattern shows a mixture of extra lines of both the higher and the lower stage structures.

In the stepwise debromination process of $C_{16}Br_2$, the 3rd, 4th and 5th stages appear in that order. However, the equilibrium vapor pressures are much lower than those for the bromination process. This is due to the tendency for the retention of bromine in the compound. After the vapor pressure of bromine is reduced to zero, a residue compound remains.

The understanding of the structure of the residue compounds is much more limited than that of the lamellar compounds. There are two possible ways in which the intercalates are retained in the residue compounds:

(1) intercalate layers are trapped between the carbon layers, as in lamellar compounds, and (2) intercalate is trapped at imperfections in the graphite crystal lattice.

9.4.2. Graphite-alkali metals

Graphite-alkali metals belong to the class of "ionic" intercalation compounds. They are n-type, whereas the graphite-halogens (Sec. 9.4.1) are p-type.

The alkali metal intercalates include Li, Na, K, Rb and Cs. The compounds of K, Rb and Cs behave quite similarly and are all different from those of Li and Na. The compounds of K, Rb and Cs have stoichiometries C_8X, $C_{24}X$, $C_{36}X$, $C_{48}X$ and $C_{60}X$ (X = K, Rb or Cs), which correspond to stages 1, 2, 3, 4 and 5 respectively [67], although stage 1 compounds with intercalate concentration exceeding that of C_8X have been reported [68, 69]. The Li compounds include C_6Li, $C_{12}Li$ and $C_{18}Li$, which correspond to stages 1, 2 and 3 respectively [70, 71]. In addition to the binary graphite-alkali metal systems, there are ternary systems which involve two different alkali metals [67].

The differences between the alkali metals in their behavior toward graphite can be explained in various ways, though none of the ways has accounted for all the differences. One explanation is in terms of the size effect. The nearest neighbor distances in the alkali metals are 5.25, 4.86, 4.62, 3.68, 3.00 Å, going from Cs to Li. These distances in the pure metals can be compared to those in the compound. Consider, for instance, the stage 1 compound C_8X (X = K, Rb, Cs). The nearest neighbor distance is more or less fixed by the graphite lattice at 4.91 Å. Thus one can see that K fits into the graphite lattice slightly more loosely than into K metal; Rb fits perfectly; and Cs is somewhat squeezed. The nearest neighbor distance in the metals Na and Li are much smaller than 4.91 Å. This may be the reason why Na does not intercalate readily and Li intercalates in a different way (C_6Li instead of C_8Li). The denser packing of the alkali metals in the C_6X structure than in the C_8X structure is consistent with the small size of the Li atom.

There are several methods to prepare lamellar compounds of graphite-alkali metals. In one method, graphite is heated with weighed quantities of the alkali metal in an evacuated vessel. In the second method, known as the two-bulb method [72], the alkali metal and the graphite are in two bulbs typically held at 250°C and 250–600°C respectively. The greater the temperature difference between the two bulbs, the lower is the intercalate concentration in the resulting compound. The saturated compound C_8X (X = K, Rb, Cs) can be obtained by holding both bulbs at the same temperature. Stages 4, 3, 2 and 1 can be formed successively within a single graphite sample. The third method involves electrochemical intercalation [73–77], which is relevant to Li-ion secondary batteries [78].

The effects of alkali metal (K, Rb, Cs) intercalation on the electrical properties of graphite are summarized below:

(a) decrease in the electrical resistivity in both a and c axes,

10

(b) decrease in anisotropy ratio of electrical resistivity,

(c) increase in the positive temperature coefficient of electrical resistivity in both a and c axes,

(d) change in sign of the thermoelectric power in both a and c axes,

(e) decrease in the negative Hall coefficient with increasing intercalate concentration,

(f) anomalies in the electrical conductivity in the temperature range 77–360°K.

The electrical resistivity in both a and c axes are decreased on intercalation but the decrease in the c-axis is more pronounced. Whereas the c-axis resistivity decreases continuously with increasing content of alkali metal, a limiting decrease in the direction of the a-axis appears to be reached at ~stage 4 [79].

The effects of alkali metal intercalation on the magnetic properties of graphite are summarized below:

(a) change of the magnetic susceptibility from negative to positive,

(b) changes in the g-shift and the linewidth of the electron spin resonance,

(c) Knight shift of the Cs^{133} nuclear magnetic resonance.

There are numerous ternary compounds involving the alkali metals and other species (e.g., oxygen, benzene and halide) [80–84].

9.4.3. Graphite-acid compounds

Graphite react with a large number of acids to form intercalation compounds which have been referred to as "acid salts of graphite". They have received much interest because of their high electrical conductivities. The acid intercalates include nitric acid (HNO_3), sulfuric acid (H_2SO_4), perchloric acid ($HClO_4$), selenic acid (H_2SeO_4), etc. [85, 86]. These acids act as electron acceptors in the graphite crystal by forming negatively charged acids radicals (NO_3^-, HSO_4^-, etc.). However only a fraction of the acid molecules undergoes this ionization. The rest remains as acid molecules in the graphite crystal. Graphite-HNO_3 (also known as graphite nitrate) and graphite-H_2SO_4 (also known as graphite bisulfate) are the most extensively studied compounds in this category.

Graphite nitrate can be prepared by direct chemical interaction of graphite with nitric acid [87] or be electrolysis [88]. The chemical method involved nitration in the liquid or vapor phase. In liquid-phase nitration, graphite is immersed in nitric acid (HNO_3) of various acid strengths. Stage 1 compounds can be obtained by use of a mixture of 50% of fuming nitric acid (s.g. 1.52) by weight with 50% of nitrogen pentoxide (N_2O_5) directly prepared by distillation from nitric acid and phosphorus pentoxide (P_2O_5). The stage 1 compounds are blue. All higher stages can be obtained without nitrogen pentoxide. Stage 2 compounds can be obtained by use of fuming nitric acid.

In vapor-phase nitration, graphite is exposed to nitric acid vapor of various partial pressures. More

satisfactory samples can be obtained by vapor-phase nitration than by liquid-phase nitration because liquid-phase nitration proceeds so rapidly at the edges of the sample that the edges swell as a result of intercalation before the molecules have time to penetrate into the interior of the layers.

The electrochemical method involves the use of graphite as reference electrode and fuming nitric acid as electrolyte [88].

Graphite bisulfate consists of graphite layers with HSO_4^- ions and H_2SO_4 molecules between the layers.

The blue stage 1 graphite bisulfate lamellar compound can be prepared by direct chemical interaction of graphite with a mixture of concentrated sulfuric acid and an oxidizing agent (nitric acid, chromic oxide, potassium permanganate, ammonium persulfate, manganese dioxide, lead dioxide, arsenic pentoxide, iodic acid, periodic acid or manganese salts) or by electrolysis [61, 89–92].

The advantage of the electrochemical method of sample preparation is that the number of anions intercalated can be evaluated by applying Faraday's law. This allows the determination of n in the chemical formula $C_nHSO_4 \cdot xH_2SO_4$. By weight uptake measurement, the value of x can be obtained if n is known. The occurrence of stages gives rise to steps in the curve of the electrode potential vs. current or time. Together with the X-ray diffraction results, these steps indicate that $n = 24$ in stage 1 and $n = 48$ in stage 2 [62, 88]. The value of x is 2.5 [93] in both stages 1 and 2.

When a small amount of water is added to the sulfuric acid, the blue compound decomposes in a step-wise manner into mixtures of higher stage lamellar compounds [87] which are not blue (e.g., pure graphite is silvery). The decomposition also occurs by exposing the blue compound to air [94]. The blue color is lost soon after exposure to air, although X-ray diffraction still shows the presence of some amount of the first stage lamellar compound [95]. The decomposition in air is due to the absorption of water.

9.4.4. Graphite-halide compounds

Graphite forms intercalation compounds with a large number of halides. The halogens involved include F, Cl, Br and I. Most of the halides investigated are chlorides, though the fluorides are receiving attention. The halides act as electron acceptors in graphite.

Graphite-ferric chloride is the best studied graphite-metal halide partly because it is the oldest and partly because of its interesting magnetic properties.

Graphite-ferric chloride lamellar compounds of stage 1 (69 wt%), stage 2 (53 wt%), stage 3 (42 wt%), stage 4 (35 wt%), stage 5 (30 wt%) and stage 6 (28 wt%) have been obtained [96–98].

Graphite-ferric chloride has been prepared by heating graphite with anhydrous $FeCl_3$ [96]. After cooling the product, the excess $FeCl_3$ is removed by either washing with hydrochloric acid or sublimation. By varying the reaction temperature, which is above 180°C, different stages can be obtained. The graphite sample is usually maintained at a higher temperature than the $FeCl_3$ to minimize the condensation of $FeCl_3$

sample. Graphite-ferric chloride is p-type. A less common method involves electrochemical intercalation [99].

Graphite-antimony pentafluoride has received attention due to the high in-plane electrical conductivity [100]. The stage 1 compound is blue black. All higher stage compounds are black [101].

10. Exfoliated graphite

Graphite intercalation compounds tend to exfoliate upon heating [4]. The exfoliation involves a large expansion (by as many as several hundred times) along the c-axis. It is due to the tendency of the intercalate in the graphite to vaporize, thus forming gas pockets which may or may not burst. The expansion of the gas pockets is made possible by the shear of the graphite layers with respect to one another. If the pockets do not burst and the heating is not excessive, the exfoliation can be reversible upon subsequent cooling. However, excessive heating causes irreversible exfoliation.

Exfoliation is most commonly conducted on intercalated graphite in the form of flakes, as a graphite flake has the graphite layers aligned in the plane of the flake and expansion along the c-axis is not hindered by ~~geometry~~. After irreversible exfoliation, the flake is much longer along the c-axis than in the in-plane direction, so it is referred to as a worm. The macroporosity of exfoliated graphite is attractive for biomedical applications [102].

geometry.

Compression of a collection of worms without a binder results in mechanical interlocking among the worms. Thus, a flexible sheet (called flexible graphite) is formed [5]. The worms used for making flexible graphite are preferably those that have been made by exfoliation that involves bursting of the gas pockets. The sheet is resilient and can be cut by using scissors. It is commonly used as a gasket material for harsh environments, since graphite is rather inert chemically and is high temperature resistant. It can also be used as a gasket material for electromagnetic interference (EMI) shielding, since its electrical conductivity and high specific surface area (typically 10–15 m^2/g) enhance the reflection of high frequency (up to GHz) electromagnetic radiation [5].

11. Carbon fibers

Carbon fibers refer to fibers which are at least 92 wt% carbon in composition. They can be short or continuous; their structure can be crystalline, amorphous, or partly crystalline. The crystalline form has the crystal structure of graphite. The high modulus of a carbon fiber stems from the fact that the carbon layers, though not necessarily flat, tend to be parallel to the fiber axis. This crystallographic preferred orientation is known as a fiber texture. As a result, a carbon fiber has a higher modulus parallel to the fiber axis than perpendicular to the fiber axis. Similarly, the electrical and thermal conductivities are higher along the fiber axis, and the coefficient of thermal expansion is lower along the fiber axis.

The greater the degree of alignment of the carbon layers parallel to the fiber axis, i.e., the stronger the fiber texture, the greater the c-axis crystallite

size (L_c), the density, the carbon content, and the fiber's tensile modulus, electrical conductivity, and thermal conductivity parallel to the fiber axis; the smaller the fiber's coefficient of thermal expansion and internal shear strength. In a carbon fiber, there can be graphite regions of size L_c perpendicular to the layers and size L_a parallel to the layers. There can also be crystalline regions in which the carbon layers, though well developed and parallel to one another, are not stacked in any particular sequence; the carbon in these regions is said to be turbostratic carbon. Yet another type of carbon that can exist in carbon fibers is amorphous carbon, in which the carbon layers, though well developed, are not even parallel to one another.

The proportion of graphite in a carbon fiber can range from 0 to 100%. When the proportion is high, the fiber is said to be graphitic, and it is called a graphite fiber. However, a graphite fiber is polycrystalline, whereas a graphite whisker is a single crystal with the carbon layer rolled up like a scroll. Because of their single crystal nature, graphite whiskers are virtually flaw-free and have exceptionally high strength. However, the production yield of graphite whiskers is too low for them to be commercially significant.

Carbon fibers that are commercially available are divided into three catagories, namely general-purpose (GP), high-performance (HP), and activated carbon fibers (ACF). The general-purpose type is characterized by an amorphous and isotropic structure, low tensile strength, low tensile modulus and low cost. The high-performance type is characterized by relatively high strength and modulus. Among the high-performance carbon fibers, a higher modulus is associated with a higher proportion of graphite and more anisotropy. Activated carbon fibers are characterized by the presence of a large number of open micropores, which act as adsorption sites. The adsorption capacity of activated carbon fibers is comparable to that of activated carbons, but the fiber shape of activated carbon fibers allows the adsorbate to get to the adsorption site faster, thus accelerating the adsorption and desorption processes. The amount adsorbed increases with the severity of activation.

Intercalation can occur in graphite fibers, i.e., carbon fibers having a high degree of crystallinity. Intercalation can be used to modify the fibers so as to increase the effectiveness for electromagnetic interference shielding [3, 5] or to increase the thermoelectric power for use of a fiber composite as thermcouples [103]. Although there is chemical reactivity between noncrystalline carbons (such as noncrystalline carbon fibers and coal) and various intercalates, the reactions do not result in a graphite intercalation compound.

12. Oxidation protection

The tendency for carbons to oxidize and become a vapor is a problem that limits the use of carbons at high temperatures. Structural carbons include carbon fibers, carbon-carbon composites and graphite. They are used in aerospace and various industrial applications. Much attention has been given to the development of methods of oxidation protection of carbon materials [104–107].

The dominant method of oxidation protection of carbons involves the use of a coating, such as SiC [108–129], silicon oxycarbide [130], TiC [131], TiN [132], TiO_2 [133, 134], Si_3N_4 [135, 136], B_4C [137, 138], SiO_2 [139], $ZrSiO_4$ [140, 141], ZrO_2 [142], Si-Hf-Cr [143], Al_2O_3 [144–146], Al_2O_3-SiO_2 [147, 148], SiC/C [149–154], BN [155–157], Si-B [158, 159], mullite [160–162], LaB_6 [163], $MoSi_2$ [164], Y_2SiO_5 [165–168] and glass [169–171]. These ceramic coatings are mostly applied by either chemical vapor deposition (CVD) or pyrolysis of a preceramic polymer [172, 173].

Another method of oxidation protection of carbons involves surface treatment with a reactive aqueous solution [174], such as phosphoric acid [175, 176], oxifluoride phosphate compounds [177], $POCl_3$ [178] and boric acid [179]. Immersion in the solution is followed by drying and sometimes heating as well. This method should be distinguished from the formation of a ceramic coating by dipping in a sol-gel [180]. The solution technique is simple compared to CVD, though it usually provides oxidation protection in a lower temperature range than the ceramic coating method [174].

13. Activated carbon

Activated carbon refers to a carbon material that has surface porosity which results in a specific surface area typically exceeding 1000 m^2/g. The pores are typically micropores (below 20 Å in size), although mesopores (above 20 Å in size) are abundant in activated carbons that have been suitably prepared [181, 182]. Activated carbon is used for the adsorption of molecules and ions for the purpose of water treatment, air purification, gas separation, solvent recovery, odor revoval and related applications that are relevant to environmental engineering [183, 184].

Activated carbon is typically made by heating a carbon precursor (e.g., pitch and polyacrylonitrile) or a carbon material in a reactive atmosphere. The process, known as activation, is a reaction (such as C + $CO_2 \rightarrow$ 2CO) which changes some of the material into vapor, thereby resulting in surface pores. Activation is relatively difficult if the carbon material has been graphitized prior to activation. A pre-treatment involving ozone serves to increase the surface oxygen concentration, thereby facilitating activation [185].

14. Conclusion

Graphite is an engineering material that is rich in physics and chemistry, in addition to being useful in bulk, fibrous, activated and exfoliated forms. However, oxidation protection is required for high temperature applications.

References

1. M. INAGAKI, *Nihon Enerugi Gakkaishi/Journal of the Japan Institute of Energy* 77(9) (1998) 857.

2. M. S. DRESSELHAUS and G. DRESSELHAUS, in Proc. 7th International Symposium on Intercalation Compounds, Molecular Crystals & Liquid Crystals Science & Technology Section A—Molecualr Crystals & Liquid Crystals (1994) Vol. 244, p. 1.

3. G. HARRIS, J. LENNHOFF, J. NASSIF, M. VINCIGUERRA, P. ROSE, D. JAWORSKI and

J. GAIER, in Proc. 1999 31st International SAMPE Technical Conf., Advanced Materials and Processes Preparing for the New Millennium (1999) Vol. 31, p. 122.

4. D. D. L. CHUNG, *J. Mater. Sci.* 22(12) (1987) 4190.

5. *Idem., J. Mater. Eng. Perf.* 9(2) (2000).

6. J. D. BERNAL, *Proc. Roy. Soc.* A106 (1924) 749.

7. R. W. G. WYCKOFF, "Crystal Structures," Vol. 1 (Interscience, New York, 1963).

8. W. RULAND, "Chemistry and Physices of Carbon," edited by Walker and Thrower (1968) Chapter 4.

9. L. J. BRILLSON, E. BURSTEIN, A. A. MARADUDIN and T. STARK, "The Physics of Semimetals and Narrow Gap Semiconductors," edited by Carter and Bate (Pergamon Press, NewYork, 1971) p. 187.

10. H. LIPSON and A. R. STOKES, *Proc. Roy. Soc.* A227 (1942) 330.

11. H. JAGODZINSKI, *Acta Cryst.* 2 (1949) 298.

12. R. R. HAERING, *Can. J. Phys.* 36 (1958) 352.

13. J. W. McCLURE, *Carbon* 7 (1969) 425.

14. G. E. BACON, *Acta Cryst.* 3 (1950) 20.

15. H. P. BOEHM and U. HOFMANN, *Z. Anorg. u. Allgem. Chem.* 278 (1955) 58.

16. *Idem., ibid.* 278 (1955) 299.

17. W. P. EATHERLY, private communications, 1975.

18. A. W. MOORE, *Ned. Tijdschrift Natuurkde* (Netherlands) 32(7) (1966) 221.

19. *Idem.* in "Chemistry and Physics of Carbon," edited by P. L. Walker, Jr. (Dekker, New York, 1973) Chapter 11, p. 69.

20. J. C. SLONCZEWSKI and P. R. WEISS, *Phys. Rev.* 109 (1958) 272.

21. J. W. McCLURE, *ibid.* 108 (1957) 612.

22. M. S. DRESSELHAUS, G. DRESSELHAUS and J. E. FISCHER, *ibid.* B15 (1977) 3180.

23. P. R. SCHROEDER, M. S. DRESSELHAUS and A. JAVAN, in "The Physics of Semimetals and Narrow Gap Semiconductors" edited by Carter and Bate (Pergamon Press, New York, 1971) p. 139.

24. B. L. HEFLINGER, M. S. thesis, Department of Electrical Engineering, Massachusetts Institute of Technology, Cambridge, MA, USA, 1971.

25. W. W. TOY, M. S. DRESSELHAUS and G. DRESSELHAUS, *Phys. Rev.* B15 (1977).

26. I. L. SPAIN, in "Chemistry and Physics of Carbons," edited by Walker and Thrower (1973) Vol. 8, Chapter 1.

27. J. W. McCLURE, in "The Physics of Semimetals and Narrow Gap Semiconductors," edited by Carter and Bate (Pergaman Press, New York, 1971) p. 127.

28. *Idem., Phys. Rev.* 119 (1960) 606.

29. M. INOUE, *J. Phys. Soc. Japan* 17 (1962) 808.

30. P. R. SCHROEDER, Ph.D. thesis, Department of Physics, Massachusetts Institute of Technology, Cambridge, MA, U.S.A, 1969.

31. G. F. DRESSELHAUS, *Phys. Rev.* B10 (1974) 3602.

32. I. L. SPAIN, A. R. UBBELOHDE and D. A. YOUNG, *Phil. Trans. Roy. Soc.* (London) A262 (1967) 1128.

33. L. J. BRILLSON, Ph.D. thesis, Department of Physics, University of Pennsylvania, Philadelphia, PA, USA, 1972.

34. F. TUINSTRA and J. L. KOENIG, *J. Chem. Phys.* 53 (1970) 1126.

35. R. A. FRIEDEL and G. L. CARLSON, *J. Phys.* C 75 (1971) 1149.

36. R. NICKLOW, N. WAKABAYASHI and H. G. SMITH, *Phys. Rev.* B5 (1972) 4951.

37. J. J. SONG, D. D. L. CHUNG, P. C. EKLUND and M. S. DRESSELHAUS, *Solid State Comm.* 20 (1976) 1111.

38. G. HERZBERG, "Molecualr Spectra and Molecular Structure" (Van Nostrand, New York, 1950).

39. R. J. NEMANICH and S. A. SOLIN, *Solid State Comm.* 23(7) (1977) 417.

40. G. R. HENNIG, in "Proc. of the 2nd Carbon Conf. (Pergaman Press, Oxford, 1956) p. 103.

41. H. L. RILEY, *Fuel* 24 (1945) 8; *Idem., ibid.* 24 (1945) 24.

42. G. R. HENNIG, in "Progr. Inorg. Chem.," edited by F. A. Cotton (Wiley Interscience, New York, 1959) Chapter 1, p. 125.

43. W. RUDORFF, *Adv. Inorg. Chem. Radiochem.* **1** (1959) 223.

44. R. C. CROFT, *Q. Rev.* **XIV** (1960) 1.

45. L. B. EBERT, *Ann. Rev. Mat. Sci.* **6** (1976)181.

46. M. ASANO, T. SASAKI, T. ABE, Y. MIZUTANI and T. HARADA, *J. Phy. & Chem. Solids* **57** (1996) 787.

47. C. T. HO and D. D. L. CHUNG, *Carbon* **28**(6) (1990) 825.

48. G. R. HENNIG, *J. Chem. Phys.* **20** (1952) 1438.

49. U. HOLFMANN and R. HOLST, *Berichten* **72** (1939) 754.

50. O. RUFF, D. BRETSCHREIDER and F. EBERT, *Z. Anorg. u. Allgem. Chem.* **217** (1934) 1.

51. R. J. LAGOW, R. B. BADACHHAPE, J. L. WOOD and J. L. MARGRAVE, *Chem. Soc. Dalton* (1974) 1268.

52. T. NAKAJIMA, M. KOH, V. GUPTA, B. ZEMVA and K. LUTAR, *Electrochimica Acta* **45**(10) (2000) 1655.

53. L. B. EBERT, J. I. BRAUMAN and R. A. HUGGINS, *J. Am. Chem. Soc.* **96** (1974) 7841.

54. D. E. PALIN and K. D. WADSWORTH, *Nature* **162** (1958) 925.

55. W. RUDORFF and G. RUDORFF, *Z. Anorg. u. Allgem. Chem.* **253** (1947) 281.

56. A. M. PANICH, *Synthetic Metals* **100**(2) (1999) 169.

57. R. J. LAGOW, L. A. SHIMP, D. K. LAM and R. F. BADDOUR, *Inorg. Chem.* **11** (1972) 2568.

58. F. R. M. McDONNELL, R. C. PINK and A. R. UBBELOHDE, *J. Chem. Soc.* (1951) 191.

59. T. SASA, Y. TAKAHASHI and T. MUKAIBO, *Carbon* **9** (1971) 407.

60. G. A. SAUNDERS, A. R. UBBELOHDE and D. A. YOUNG, *Proc. Roy. Soc.* **A271** (1963) 499.

61. W. RUDORFF and U. HOFMANN, *Z. Anorg. u. Allgem. Chem.* **238** (1938) 1.

62. L. C. F. BLACKMAN, J. F. MATHEWS and A. R. UBBELOHDE, *Proc. Roy. Soc.* (London) **A258** (1960) 329.

63. G. R. HENNIG, *J. Chem. Phys.* **20** (1952) 1443.

64. W. RUDORFF, V. SILS and R. ZELLER, *Z. Anorg. Allgem. Chem.* **283** (1956) 299.

65. D. D. L. CHUNG, *Phase Transitions* **8** (1986) 35.

66. S. HIGAI, S. MIZUNO, S. SUZUKI and K. NAKAO, in Proc. 1998 9th International Symposium on Intercalation Compounds, Molecular Crystals & Liquid Crystals Science & Technology Section A—Molecular Crystals & Liquid Crystals (1998) Vol. 310, p. 267.

67. D. GUERARD, P. LAGRANGE, A. HEROLD and F. ROUSSEAUX, *Synthetic Metals* **23**(1–4) (1988); *Idem.*, in Graphite Intercalation Compd., Proceedings of the 4th International Symposium (1987) p. 421.

68. C. HEROLD, M. EL GADI, J.-F. MARECHE and P. LA GRANGE, in Proceedings of the 7th International Symposium on Intercalation Compounds, Molecular Crystals & Liquid Crystals Science & Technology, Section A—Molecular Crystals & Liquid Crystals (1994) Vol. 244, p. 41.

69. I. A. UDOD, *Synthetic Metals* **88**(2) (1997) 127.

70. A. FUNABIKI, M. INABA, T. ABE and Z. OGUMI, *J. Electrochem. Soc.* **146**(7) (1999) 2443.

71. R. JUZA and V. WHELE, *Natw.* **52** (1965) 560.

72. W.-C. OH, S.-J. CHO and Y.-S. KO, *Carbon* **34**(2) (1992) 209.

73. K. GUERIN, A. FEVRIER-BOUVIER, S. FLANDROIS, M. COUZI, B. SIMON and P. BIENSAN, *J. Electrochem. Soc.* **146**(10) (1999) 3660.

74. D. BILLAUD, L. THEVENOT and P. WILLMANN, *Electrochimica Acta* **45**(1) (1999) 59.

75. Y.-C. CHANG and H.-J. SOHN, *J. Electrochem. Soc.* **147**(1) (2000) 50.

76. C. SIMONNARD, A. METROT and P. WILLMANN, in Proceedings of the 10th International Symposium on Intercalation Compounds, Molecular Crystals & Liquid Crystals Science & Technology, Section A—Molecular Crystals & Liquid Crystals (2000) Vol. 340, p. 461.

77. C. WANG, I. KAKWAN, A. J. APPLEBY and F. E. LITTLE, *J. Electroanalytical Chem.* **489**(1) (2000) 55.

78. M. ENDO, C. KIM, K. NISHIMURA, T. FUJINO and K. MIYASHITA, *Carbon* **38**(2) (2000) 183.

79. L. C. F. BLACKMAN, J. F. MATHEWS and A. R. UBBELOHDE, *Proc. Roy. Soc.* (London) **A258** (1960) 339.

80. A. HEROLD, J.-F. MARECHE and M. LELAURAIN, *Carbon* **38**(14) (2000) 1955.

81. H. SHIOYAMA, Y. WAKUKAWA and Y. SAWADA, in Proc. 1998 9th International Symp. Intercalation Compounds, Molecualr Crystals & Liquid Crystals Science & Technology Section A—Molecular Crystals & Liquid Crystals (1998) Vol. 310, p. 69.

82. T.-R. PARK, *Solid State Comm.* **106**(8) (1998) 523.

83. H. OGATA, S. MIYAJIMA, K. MATSUTSUJI and T. ENOKI, *J. Phys. & Chem. of Solids* **57**(6–8) (1996) 703.

84. S. A. SOLIN and H. ZABEL, *Adv. Phys.* **37**(2) (1988) 87.

85. A. M. ZIATDINOV and N. M. MISHCHENKO, *Solid State Comm.* **97**(12) (1996) 1085.

86. D. ALLIATA, R. KOTZ, O. HAAS and H. SIEGENTHALER, *Langmuir* **15**(24) (1999) 8483.

87. W. RUDORFF, *Z. Phys. Chem.* **B45** (1939) 42.

88. M. J. BOTTOMLEY, G. S. PARRY, A. R. UBBELOHDE and D. A. YOUNG, *J. Chem. Soc.* (1963) 5674.

89. P. SCHAFHAUTL, *J. Prakt. Chem.* **21** (1841) 155.

90. L. E. A. BERLOUIS and D. J. SCHIFFRIN, *J. Applied Electrochem.* **13**(2) (1983) 147.

91. H. THIELE, *Z. Anorg. u. Allgem. Chem.* **206** (1932) 407.

92. G. R. HENNIG, *J. Chem. Phys.* **19** (1951) 922.

93. S. ARONSON, C. FRISHBERG and G. FRANKL, *Carbon* **9** (1971) 715.

94. A. FRENZEL and U. HOFMANN, *Z. Elektrochem. Angew. Phys. Chem.* **40** (1934) 511.

95. M. INAGAKI, *Carbon* **4** (1966) 137.

96. H. THIELE, *Z. Anorg. u. Allgem. Chem.* **207** (1932) 340.

97. W. RUDORFF and H. SCHULZ, *ibid.* **245** (1940) 121.

98. W. METZ and D. HOHLWEIN, *Carbon* **13** (1975) 84; *Idem.*, *ibid.* **13** (1975) 87.

99. F. KANG, Y. LENG, T.-Y. ZHANG and B. LI, *ibid.* **36**(4) (1998) 383.

100. M. BAXENDALE, V. Z. MORDKOVICH and S. YOSHIMURA, *Solid State Comm.* **107**(4) (1998) 165.

101. J. MELIN and A. HEROLD, *C.R. Hebd. Seances Acad. Sci. Ser.* **C280** (1975) 641.

102. W. SHEN, S. WEN, N. CAO, L. ZHENG, W. ZHOU, Y. LIU and J. GU, *Carbon* **37**(2) (1999) 356.

103. S. WANG and D. D. L. CHUNG, *Composite Interfaces* **6**(6) (1999) 519.

104. G. R. ST PIERRE, *Metallurgia Italiana* **85**(10) (1993) 603.

105. J. R. STRIFE, in "Winter Annual Meeting of the American Society of Mechanical Engineers Part 1: Damage and Oxidation Protection in High Temperature Composites" (1991) Vol. 25-1, p. 121.

106. X. YUAN, L. CHENG and L. ZHANG, *Xibei Gongye Daxue Xuebao/Journal of Northwestern Polytechnical University* **16**(4) (1998) 632.

107. Y. V. DZYADIKEVICH and V. E. OLEJNIK, *Poroshkovaya Metallurgiya* (3/4) (1996) 41.

108. L. F. CHENG, Y. XU, L. ZHANG and X. YIN, *Carbon* **38**(10) (2000) 1493.

109. T. H. ASHLEY and O. O. OCHOA, *Compos. Sci. & Tech.* **59**(13) (1999) 1959.

110. A. OTSUKA, K. SAKAMOTO and H. MASUMOTO, *Mater. Sci. Res. Int.* **5**(3) (1999) 163.

111. S.-J. PARK, J.-G. HAN and J.-H. BOO, in 42nd Annual Technical Conference Proceedings (1999) 368.

112. Q. ZHU, X. QIU and C. MA, *Carbon* **37**(9) (1999) 1475.

113. T. AOKI and H. HATTA, *Zairyo to Kankyo/Corrosion Eng.* **48**(3) (1999) 123.

114. N. S. JACOBSON, T. A. LEONHARDT, D. M. CURRY and R. A. RAPP, *Carbon* **37**(3) (1999) 411.

115. Q. GUO, J. SONG, L. LIU and B. ZHANG, *ibid.* **37**(1) (1999) 149.

116. H. HATTA, E. SUDO, Y. KOGO and I. SHIOTA, *Nippon Kinzoku Gakkaishi/J. Japan Inst. Metals* **62**(9) (1998) 861.

117. L. CHENG, L. ZHANG, Y. XU and M. LI, *Xibei Gongye Daxue Xuebao/J. Northwestern Polytechnical University* **16**(1) (1998) 129.

118. Q. ZHU, X. QIU and C. MA, *Qinghau Daxue Xuebao/J. Tsinghua University* **37**(6) (1997) 58.

119. Y. KOGO, H. HATTA, A. OKURA, Y. GOTO, Y. SAWADA, Y. OYA-SEIMIYA, *et al.*, *Nippon Kinzoku Gakkaishi/J. Japan Inst. Metals* **62**(2) (1998) 197.

120. L. CHENG, L. ZHANG and Y. XU, *Cailiao Yanjiu Xuebao/Chinese J. Mater. Res.* **10**(6) (1996) 665.

121. C.-C. M. MA, N.-H. TAI, W.-C. CHANG and H.-T. CHAO, *J. Mater. Sci.* **31**(3) (1996) 649.

122. A. SAKAI, N. KITAMORI, K. NISHI and S. MOTOJIMA, *Mater. Letters* **25**(1/2) (1995) 61.

123. H. T. TSOU and W. KOWBEL, *Carbon* **33**(9) (1995) 1279.

124. Y.-Q. WANG, Z.-M. WANG, J.-Y. YANG, F.-Q. ZHANG and B.-L. ZHOU, *Compos. Manufacturing* **6**(2) (1995) 103.

125. F. LAMOUROUX, X. BOURRAT, R. NASLAIN and J. THEBAULT, *Carbon* **33**(4) (1995) 525.

126. Y.-Q. WANG, B.-L. ZHOU and Z.-M. WANG, *ibid.* **33**(4) (1995) 427.

127. S. CHU, H. WANG and G. HE, *Wuji Cailiao Xuebao/J. Inorganic Mater.* **8**(3) (1993) 327.

128. P. E. GRAYSON and N. J. ARCHER, in 17th Annual Conference on Composites and Advanced Ceramic Materials (1993) Vol. 14(9/10) pt. 2, p. 832.

129. D. KEHR, K. BRENNFLECK and R. WEISS, *High Temp.— High Pressures* **22**(6) (1990) 693.

130. M. HARRIS, T. CHAUDHARY, L. DRZAL and R. M. LAINE, *Mater. Sci. & Eng. A: Structural Mater.: Properties, Microstructure & Processing* 1/2 (1995) 223.

131. C. KAWAI and T. IGARASHI, *J. Ceramic Soc. Japan, Int. Ed.* **99**(5) (1991) 377.

132. Y. LIU, D. R. TREADWELL, M. R. KANNISTO, B. L. MUELLER and R. M. LAINE, *J. Amer. Ceram. Soc.* **80**(3) (1997) 705.

133. J. YU, S. YENO and K. HIRAGUSHI, *Nippon Seramikkusu Kyokai Gakujutsu Ronbunshi/J. Ceramic Soc. Japan* **104**(1210) (1996) 481.

134. T. HASHISHIN, J. MURASHITA, A. JOYAMA and Y. KANEKO, *ibid.* **106**(1229) (1998) 1.

135. H. T. TSOU and W. KOWBEL, *Carbon* **33**(9) (1995) 1289.

136. Y.-C. ZHU, S. OHTANI, Y. SATO and N. IWAMOTO, *ibid.* **37**(9) (1999) 1417.

137. H. T. TSOU and W. KOWBEL, *J. Adv. Mater.* **27**(3) (1996) 9.

138. K. KOBAYASHI, K. MAEDA, H. SANO and Y. UCHIYAMA, *Carbon* **33**(4) (1995) 397.

139. W. P. HOFFMAN, H. T. PHAN and A. GROSZEK, in TMS Materials Week 94 Symposium, High Temperature High Performance Materials for Rocket Engines and Space Applications, (1994) 141.

140. O. YAMAMOTO, T. SASAMOTO and M. INAGAKI, *Carbon* **33**(4) (1995) 359.

141. L. M. MANOCHA and S. M. MANOCHA, *ibid.* **33**(4) (1995) 435.

142. V. K. PARASHAR, V. RAMAN and O. P. BAHL, *J. Mater. Sci. Letters* **16**(6) (1997) 479.

143. A. JOSHI and J. S. LEE, *Composites—Part A: Applied Science & Manufacturing* **28**(2) (1997) 181.

144. H. YOSHIMATSU, S. FUJIWARA, R. KONISHI, M. MIYAWAKI and Y. MIURA, *Nippon Seramikkusu Kyokai Gakujutsu Ronbunshi/J. Ceramic Soc. Japan* **103**(1201) (1995) 929.

145. Y. WANG, J. ZHENG, Z. WANG, B. ZHOU and L. ZHOU, *Fuhe Cailiao Xuebao/Acta Materiae Compositae Sinica* **12**(3) (1995) 31.

146. K. KAWABATA, H. YOSHIMATSU, K. FUJIWARA, H. MIHASHI, K. HIRAGUSHI, A. OSAKA, *et al.*, *Nippon Seramikkusu Kyokai Gakujutsu Ronbunshi/J. Ceramic Soc. Japan* **107**(1249) (1999) 832.

147. F. CAO, P. PENG and X. LI, *Fuhe Cailiao Xuebao/Acta Materiae Compositae Sinica* **16**(1) (1999) 22.

148. C. C. LANDRY and A. R. BARRON, *Carbon* **33**(4) (1995) 381.

149. W. KOWBEL, M. MUSZYNSKI and H. T. TSOU, in Winter Annual Meeting of the American Society of Mechanical Engineers Part 1, Damage and Oxidation Protection in High Temperature Composites (1991) Vol. 25-1, p. 65.

150. K. FUJII, J. NAKANO and M. SHINDO, *J. Nuclear Mater.* **203**(1) (1993) 10.

151. W. KOWBEL, J. C. WITHERS and P. O. RANSONE, *Carbon* **33**(4) (1995) 415.

152. S. CHU, H. WANG and R. WU, *Surface & Coatings Tech.* **88**(1–3) (1997) 38.

153. J. DENG, Y. WEI and W. LIU, *J. Amer. Ceram. Soc.* **82**(6) (1999) 1629.

154. R. YAMADA and K. FUJII, *Mater. Sci. Forum* **308–311** (1999) 902.

155. H. T. TSOU and W. KOWBEL, *Surface & Coatings Tech.* **79**(1–3) (1996) 139.

156. A. W. MOORE, M. B. DOWELL, E. R. STOVER and L. D. BENTSEN, *Ceramic Eng. & Sci. Proc.* **16**(4) (1995) 263.

157. C. G. COFER and J. ECONOMY, *Carbon* **33**(4) (1995) 389.

158. T.-M. WU, W.-C. WEI and S.-E. HSU, *Ceramics Int.* **18**(3) (1992) 167.

159. J. W. FERGUS and W. L. WORRELL, *Carbon* **33**(4) (1995) 537.

160. H. FRITZE, J. JOJIC, T. WITKE, C. RUESCHER, S. WEBER, S. SCHERRER, B. SCHULTRICH, *et al.*, *Key Eng. Mater.* **132–136**(3) (1997) 1629.

161. H. FRITZE, A. SCHNITTKER, T. WITKE, C. RUESCHER, S. WEBER, S. SCHERRER, *et al.*, *Mater. Res. Soc. Symp. Proc.* **555** (1999) 79.

162. O. YAMAMOTO, T. SASAMOTO and M. INAGAKI, *J. Mater. Sci. Lett.* **19**(12) (2000) 1053.

163. R. WANG, H. SANO, Y. UCHIYAMA and K. KOBAYASHI, *J. Mater. Sci.* **31**(23) (1996) 6163.

164. X. ZENG, H. LI, Z. YANG and X. ZHU, *Chinese J. Aeronautics* **12**(2) (1999) 111.

165. M. KONDO, Y. OGURA and T. MORIMOTO, *Mater. Transactions Jim.* **39**(11) (1998) 1146.

166. N. SAKAKIBARA, A. NOTOMI, Y. OGURA, M. KONDO, C. FUJIWARA, T. SEKIGAWA, *et al.*, *Nippon Kinzoku Gakkaishi/J. Japan Inst. Metals* **63**(1) (1999) 118.

167. M. KONDO, Y. OGURA and T. MORIMOTO, *ibid.* **63**(5) (1999) 661.

168. M. KONDO, Y. OGURA, T. MORIMOTO and A. NOTOMI, *ibid.* **63**(7) (1999) 851.

169. M. GUO, K. SHEN and Y. ZHENG, *Carbon* **33**(4) (1995) 449.

170. F. J. BUCHANAN and J. A. LITTLE, *ibid.* **33**(4) (1995) 491.

171. N. E. LOBIONDO, L. E. JONES and A. G. CLARE, *ibid.* **33**(4) (1995) 499.

172. S. HOSHII, A. KOJIMA and S. OTANI, *J. Mater. Sci. Lett.* **19**(2) (2000) 169.

173. S. T. SCHWAB and R. C. GRAEF, in Winter Annual Meeting of the American Society of Mechanical Engineers, Part 1: Damage and Oxidation Protection in High Temperature Composites (1991) Vol. 25-1, p. 131.

174. S. LABRUQUERE, R. PAILLER, R. NASLAIN and B. DESBAT, *Key Eng. Mater.* **132–136**(3) (1997) 1938.

175. D. CHO, B. YOON II, H. S. HA and Y. S. LIM, *Polymer J.* **29** (1997) 959.

176. D. CHO, *Carbon* **39**(9) (1996) 1151.

177. P. H. VAST, *Ceramic Eng. & Sci. Proc.* **16**(5) (1995) 1063.

178. T. L. DHAMI, O. P. BAHL and B. R. AWASTHY, *Carbon* **33**(4) (1995) 479.

179. J. A. SEKHAR, J. LIU, J. LI, V. DE NORA, in 127th TMS Annual Meeting, Light Metals Light Metals (1998) p. 645.

180. J. N. STUECKER, D. A. HIRSCHFELD and D. S. MARTIN, *J. Mater. Sci.* **34**(22) (1999) 5443.

181. W. LU and D. D. L. CHUNG, *Carbon* **35**(3) (1997) 427.

182. T. KYOTANI, *ibid.* **38**(2) (2000) 269.

183. S. J. ALLEN, L. WHITTEN and G. McKAY, *Developments in Chem. Eng. & Mineral Processing* **6**(5) (1998) 231.

184. R. C. BROWN, *Int. J. Occupational Safety & Ergonomics* **1**(4) (1995) 330.

185. W. LU and D. D. L. CHUNG, *Carbon* **39**(1) (2000) 39.